ChemPubSoc Europe

DOI: 10.1002/chem.201603841

CHEMISTRY
A European Journal
Full Paper

Photoluminescent Complexes |*Hot Paper*|

Luminescent Gold(III) Thiolates: Supramolecular Interactions Trigger and Control Switchable Photoemissions from Bimolecular Excited States

Lucy Currie,[a] Julio Fernandez-Cestau,*[a] Luca Rocchigiani,[a] Benoît Bertrand,[a] Simon J. Lancaster,[a] David L. Hughes,[a] Helen Duckworth,[b] Saul T. E. Jones,[c] Dan Credgington,*[c] Thomas J. Penfold,*[b] and Manfred Bochmann*[a]

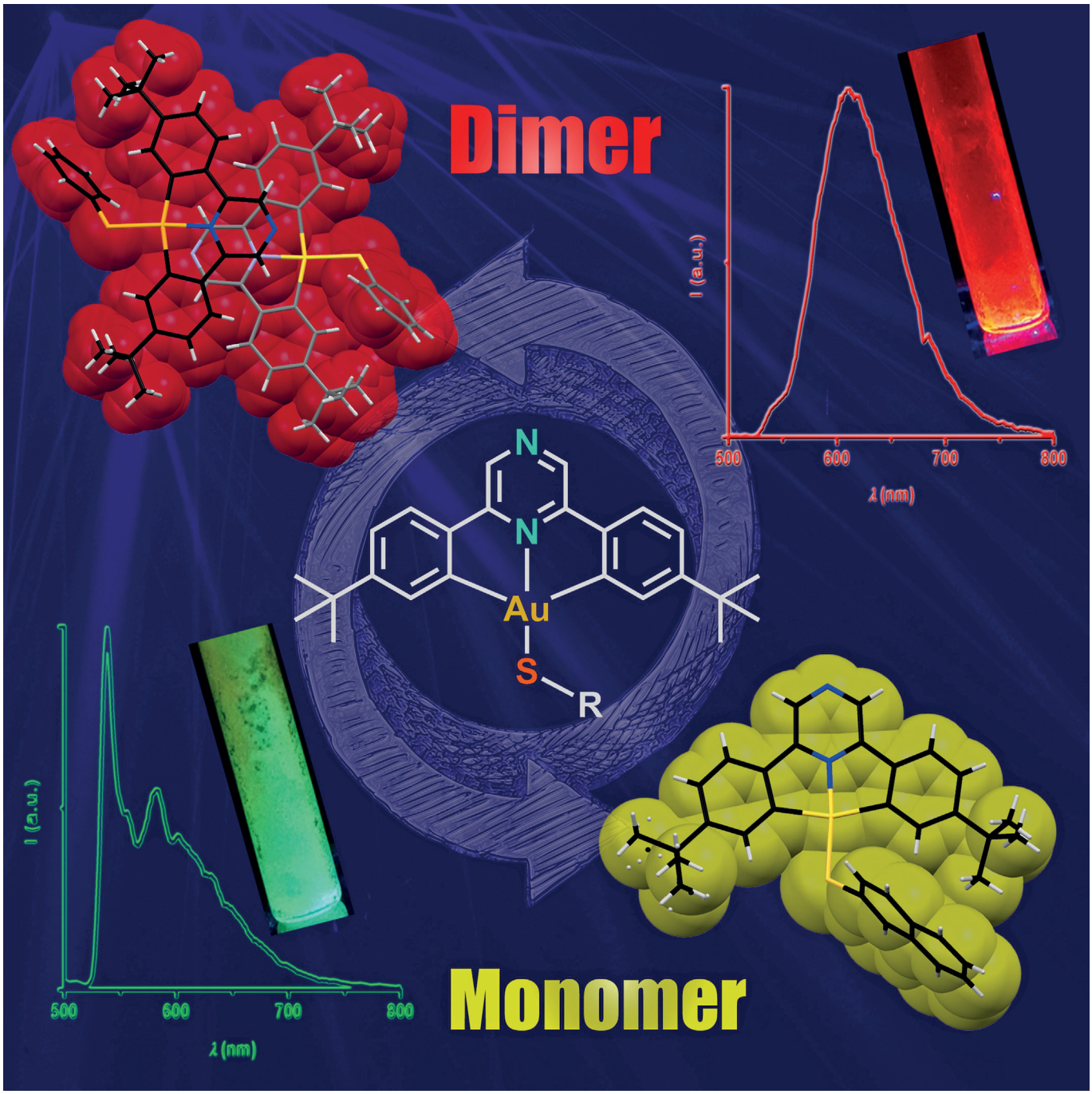

Abstract: A new family of cyclometallated gold(III) thiolato complexes based on pyrazine-centred pincer ligands has been prepared, (C^N^{pz}^C)AuSR, where C^N^{pz}^C = 2,6-bis(4-Bu^{t}C$_6$H$_4$)pyrazine dianion and R = Ph (**1**), C$_6$H$_4$*t*Bu-4 (**2**), 2-pyridyl (**3**), 1-naphthyl (1-Np, **4**), 2-Np (**5**), quinolinyl (Quin, **6**), 4-methylcoumarinyl (Coum, **7**) and 1-adamantyl (**8**). The complexes were isolated as yellow to red solids in high yields using mild synthetic conditions. The single-crystal X-ray structures revealed that the colour of the deep-red solids is associated with the formation of a particular type of short (3.2–3.3 Å) intermolecular pyrazine···pyrazine π-interactions. In some cases, yellow and red crystal polymorphs were formed; only the latter were emissive at room temperature. Combined NMR and UV/Vis techniques showed that the supramolecular π-stacking interactions persist in solution and give rise to intense deep-red photoluminescence. Monomeric molecules show vibronically structured green emissions at low temperature, assigned to ligand-based ^{3}IL(C^N^C) triplet emissions. By contrast, the unstructured red emissions correlate mainly with a ^{3}LLCT(SR→{(C^N^{pz}^C)$_2$}) charge transfer transition from the thiolate ligand to the π···π dimerized pyrazine. Unusually, the π-interactions can be influenced by sample treatment in solution, such that the emissions can switch reversibly from red to green. To our knowledge this is the first report of aggregation-enhanced emission in gold(III) chemistry.

Introduction

Gold(III) complexes stabilized by cyclometalated pincer ligands have for some years been the focus of investigation because of their photophysical properties, and for applications as sensors, as bioimaging agents, and in organic light-emitting diodes.[1–3,13] Chelating C–N bonded 2-aryl and 2,6-diaryl pyridine ligands have been found to be an effective means of stabilising Au^{III} against reduction,[4] and in combination with strong carbon-based σ-donor ligands, such as alkyl, aryl, alkynyl or N-heterocyclic carbenes (see structure **A**, where X = σ-donor ligand), they show interesting photoluminescence in solution and the solid state under ambient conditions.[5–10] The photoemissions in these cases come from pincer-ligand-based triplet states.

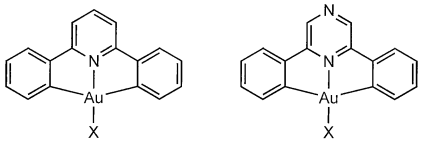

A **B**

For applications of gold(III) based luminophores the ability to modulate the emission wavelengths is of obvious importance. The most commonly applied strategies to achieve this are either the modification of the pincer ligand by more or less electron-withdrawing substituents, or the introduction of suitable substituents on the aryl or alkynyl ligands, or a combination of both. In either case, this approach requires significant synthetic effort.[5,6]

Another general strategy, which has been applied particularly successfully for photoemissive Pt^{II} complexes, is to utilize the tendency of square-planar complexes to form π-stacks which, in the case of platinum, involve metal–metal interactions and lead to concentration-dependent red-shifts.[11–13] However, although Au^{III} and Pt^{II} are isoelectronic and adopt the same square-planar coordination geometry, for Au^{III} pincer complexes there is little evidence for metal–metal interaction.[14]

As we have recently shown,[15] replacing the pyridine ring in C^N^C pincer ligands by pyrazine (structure **B**) has several important consequences: firstly, the photoluminescence intensity increases, often dramatically, and secondly, strong σ-donor ligands X are no longer required to generate luminescent complexes. The π* level in pyrazine is around 0.95 eV lower than in pyridine,[16] which enhances the π-acceptor characteristics in LLCT and MLCT processes. A much wider range of X ligands will therefore lead to photoemissive compounds.

We now find that pyrazine complexes of type **B** where X = alkyl or aryl thiolate form a new class of photoluminescent complexes, with intriguing properties. Unlike previously reported gold(III) thiolates, several of these compounds show strong photoluminescence at room temperature in the solid state, in solution, and in a polymer matrix. Rather unexpectedly, some complexes form two distinct crystal polymorphs, one of which is strongly emissive at room temperature while the other is not, apparently depending on the packing and intermolecular interactions in the crystal. In fact, it turns out that only certain

[a] *L. Currie, Dr. J. Fernandez-Cestau, Dr. L. Rocchigiani, Dr. B. Bertrand, Prof. S. J. Lancaster, Dr. D. L. Hughes, Prof. M. Bochmann*
School of Chemistry, University of East Anglia
Norwich, NR4 7TJ (United Kingdom)
(+44) 16035-92044
E-mail: J.Fernandez-Cestau@uea.ac.uk
m.bochmann@uea.ac.uk

[b] *H. Duckworth, Dr. T. J. Penfold*
School of Chemistry, Newcastle University
Newcastle upon Tyne, NE1 7RU (United Kingdom)
E-mail: Tom.Penfold@newcastle.ac.uk

[c] *S. T. E. Jones, Dr. D. Credgington*
Department of Physics, Cavendish Laboratory
Cambridge University, Cambridge CB3 0HF (United Kingdom)
E-mail: djnc3@cam.ac.uk

Supporting information (details of synthesis and characterization, X-ray crystallography, photophysical properties, theoretical calculations) and the ORCID identification number(s) for the author(s) of this article can be found under http://dx.doi.org/10.1002/chem.201603841.

specific types of π-stacking produce photoemission, and that this photoemission occurs mainly from a bimolecular excited state. Furthermore, these complexes demonstrate how π-interactions control both the luminescence pathway and the emission wavelengths, from green to red. In particular, it proved possible to switch reversibly between red and green emissions.

Results and Discussion

Synthesis and characterization

In contrast to the plethora of known Au^{I} thiolato complexes,[17] gold(III) thiolates are comparatively rare. Structurally characterized examples include compounds of the type $[X_2Au(\mu\text{-}SR)]_2$ (X = Cl, Me; R = alkyl, aryl),[18] tetrathiolato anions $[Au(SR)_4]^-$ (R = aryl or fluoroaryl),[19] polynuclear Au^{I}/Au^{III} compounds,[20] and Au^{III} thiolates supported by cyclometallated C^N and C^N^N ligands.[21] None of these are known to be photoluminescent. A thiopyridine pincer complex, [Au(C^N^{py}^C)(S-2-py)], (**A**, X = 2-thiopyridine), was described as only weakly emissive at 77 K and non-emissive at room temperature.[22] One reason for the relative rarity of Au^{III} thiolates is that in most cases thiols act as reducing agents to give gold(I) products; this was shown to occur, for example, even for N^N^N-type Au^{III} pincer complexes.[23] However, the complexes **1**–**8** reported herein proved stable to reduction by thiols and are easily accessible with very good yields by treating (C^N^{pz}^C)AuCl with the thiol in acetone in the presence of K_2CO_3 (Scheme 1). The analogous pyridine complex (C^N^{py}^C)AuSNp-2 (**9**) was prepared similarly for comparison.

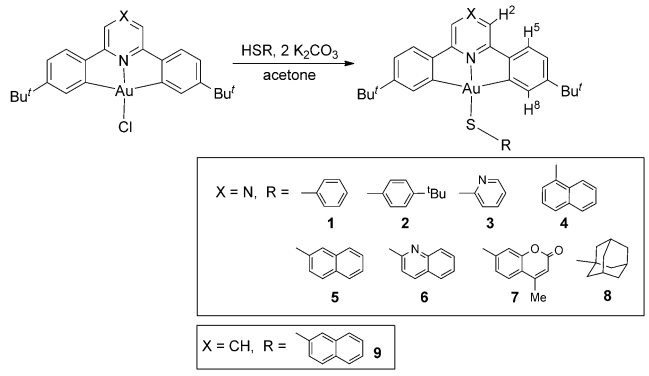

Scheme 1. Synthesis of gold(III) thiolates, including the numbering scheme used for NMR assignments.

Solid-state structure and crystal packing

Slow evaporation of a solution of (C^N^{pz}^C)AuSPh **1** in a dichloromethane/Pr^{i}OH mixture (9:1 v/v) produced two different types of crystals, red plates (**1 red**, with two independent molecules in the unit cell) together with yellow blocks (**1 yellow**). The main difference in molecular geometries between the red and yellow crystal forms are the torsion angles between the Au–S–C and S-phenyl planes, which are 50.1(4) and 58.2(3)° for the two molecules in the red form of **1**, and 94.3(6)° in the yellow form (Figure 1). Similarly, the naphthalene thiolate compound (C^N^{pz}^C)AuSNp-2 (**5**) also gave a mixture of red and yellow crystals (**5 red** and **5 yellow**, respectively; Figure 2). Here the torsion angles between the coordination plane of gold and the S-naphtyl plane in the two polymorphs are quite similar, namely 52.3(5)° (red) and 56.5(3)° (yellow). In none of these cases was this variation in crystal habit due to the inclusion of solvent molecules; the red and yellow modifications are therefore true polymorphs rather than different solvate structures.

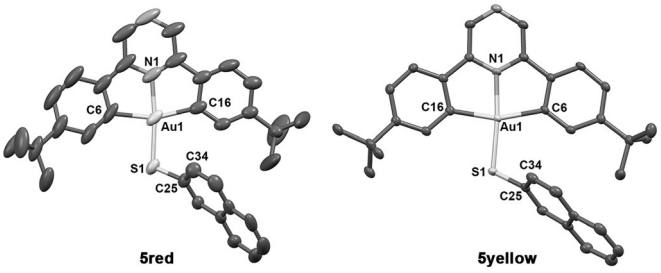

Figure 2. Left: Structure of (C^N^{pz}^C)AuSNp-2 (**5 red**).[28] Ellipsoids set at 50% probability; H atoms omitted for clarity. Selected bond distances [Å] and angles [°]: Au1–S1 2.263(2), Au1–N1 2.006(6), Au1–C6 2.069(6), Au1–C16 2.080(6); N1-Au1-S1 174.3(2), C6-Au1-N1 80.6(3), C16-Au1-N1 80.1(2), C6-Au1-S1 93.8(2), C16-Au1-S1 105.6(2), Au1-S1-C25 109.5(2), torsion Au1-S1-C25-C34 52.3(5). Right: **5 yellow**: Au1–S1 2.2837(8), Au1–N1 2.014(3), Au1–C6 2.095(3), Au1–C16 2.086(3); N1-Au1-S1 174.05(7), C6-Au1-N1 80.7(1), C16-Au1-N1 80.2(1), C6-Au1-S1 104.68(8), C16-Au1-S1 94.53(8), Au1-S1-C25 109.8(1), torsion Au1-S1-C25-C34 56.5(3).

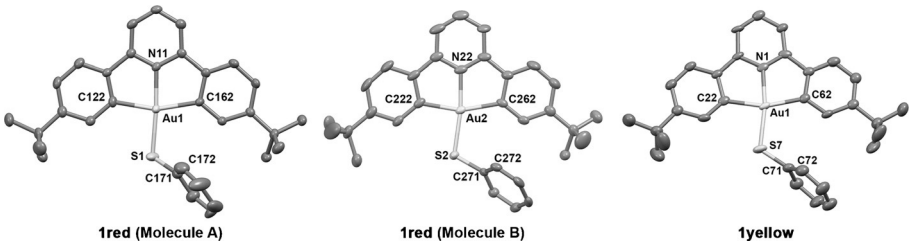

Figure 1. Structure of (C^N^{pz}^C)AuSPh (**1 red**).[28] Ellipsoids set at 50% probability; H atoms omitted for clarity. Selected bond distances [Å] and angles [°]: Molecule A: Au1–S1 2.273(1), Au1–N11 2.006(3), Au1–C122 2.086(4), Au1–C162 2.091(4); N11-Au1-S1 175.66(8), C122-Au1-N11 80.5(1), C162-Au1-N11 80.6(1), C122-Au1-S1 95.46(9), C162-Au1-S1 103.38(9), Au1-S1-C171 110.2(2), torsion Au1-S1-C171-C172 50.1(4), Molecule B: Au2–S2 2.277(1), Au2–N21 2.017(4), Au2–C222 2.083(4); N21-Au2-S2 172.2(1), C222-Au2-N21 80.6(1), C262-Au2-N21 80.1(1), C222-Au2-S2 91.8(1), C262-Au2-S2 107.49(9), Au2-S2-C271 110.9(1), torsion Au2-S2-C271-C272 58.2(3). **1 yellow**: Au1–S7 2.276(2), Au1–N1 2.022(6), Au1–C22 2.088(7), Au1–C62 2.080(7); N1-Au1-S7 170.94(18), C22-Au1-N1 81.3(3), C62-Au1-N1 79.8(3), C22-Au1-S7 89.6(2), C62-Au1-S7 109.2(2), Au1-S7-C71 116.6(3), torsion Au1-S7-C71-C72 94.3(6).

The X-ray structures of (C^N^{pz}^C)AuSC$_6$H$_4$*t*Bu-4 **2**, (C^N^{pz}^C)AuSC$_5$H$_4$N-2 **3**, (C^N^{pz}^C)AuS-4-methylcoumarin (**7**), and (C^N^{py}^C)AuSNp-2·CH$_2$Cl$_2$ (**9**·CH$_2$Cl$_2$) were also determined (see the Supporting Information). While **2** as a powder was yellow–orange, indicating a mixture of isomers, only the yellow crystals were suitable for X-ray diffraction. Compounds **3** and **7** also formed yellow crystals. The 1-naphthylthiolate **4** and the quinoline complex **6** were obtained as orange solids, while the adamantyl complex **8** was red; none gave crystals suitable for X-ray diffraction. The only compound that crystallised with a solvent molecule, CH_2Cl_2, was the pyridine-based complex **9**.

The red and yellow crystal forms of **1** and **5** show dramatic differences in their photophysical properties: the red modifications are strongly luminescent, while the yellow crystals are non-emissive at room temperature (Supporting Information, Figure S25). In the absence of compositional variation, the origin of these differences must be due to molecular interactions in the solid state.

The packing of the red and yellow forms of **1** is shown in Figure 3. Molecule A of **1 red** consists of dimers formed by a head-to-head π-interaction with pyrazine rings of neighbouring molecules adopting a "parallel offset" orientation (see the Supporting Information for the slightly different packing of molecule B).[24] The distance between the planes of the pincer ligands in these dimers is relatively short, 3.306 Å. By contrast, **1 yellow** forms one-dimensional stacks in which the pyrazine ring of one molecule is superimposed on the Au–S bond of its nearest neighbours. The *o*-phenyl protons of the PhS ligand of one molecule interact with the two pyrazine-N atoms of its neighbours forming an H···N(pz)···H rod-type arrangement. The

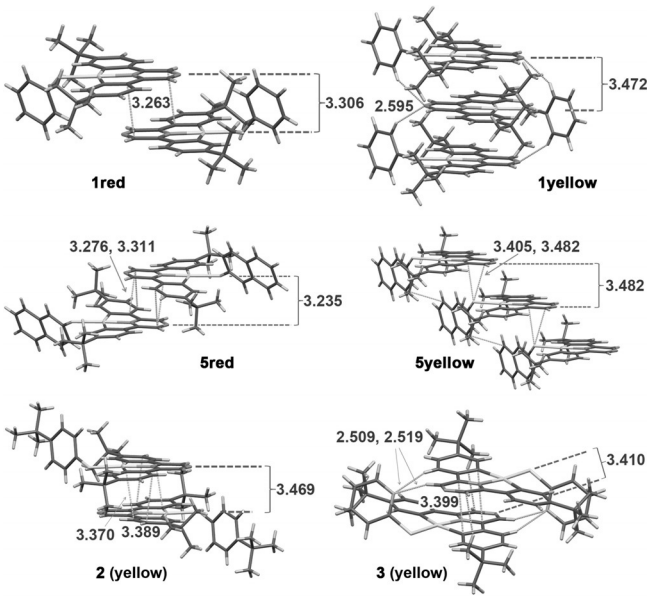

Figure 3. Intermolecular packing in emissive (red) and non-emissive (yellow) polymorphs of gold(III) thiolates, showing the pz···pz stacking of the red and pz···Au–S alignment of the yellow forms (pz = pyrazine). The inter-plane distance is measured between coordination planes of Au defined by Au, N, and C (bonded to Au). The packing diagrams of **1 yellow** and **3** also show CH···N close contacts (< 2.6 Å).

separation between molecular planes in **1 yellow** that this stacking produces is much wider than in **1 red**, 3.472 Å.

Similarly, the polymorph **5 red** shows the same type of pyrazine···pyrazine π-interactions as **1 red** and consists of π-stacked dimers with short intermolecular distances of only 3.235 Å. By contrast, the yellow isomer of this complex (**5 yellow**) crystallizes as head-to-tail rods, characterised by S···π interactions and a much wider inter-plane spacing of 3.482 Å.

The yellow crystal polymorph of (C^N^{pz}^C)AuSC$_6$H$_4$*t*Bu-4 (**2**) is also based on dimers formed through parallel offset π–π interactions, but in this case the pyrazine ring of one molecule is aligned with one of the Au–C bonds of a second molecule and vice versa, with an inter-plane distance of 3.469 Å. In the non-emissive pyridine complex **9**, a phenylpyridine moiety of one molecule is aligned with the corresponding moiety of a neighbouring molecule but avoids any direct pyridine-pyridine π-stacking.

In the 2-thiopyridine complex (C^N^{pz}^C)AuSC$_5$H$_4$N-2 (**3**) a particular case of aggregation is found as the presence of the pyridine-N atom generates intermolecular H···N···H interactions with protons of a neighbouring molecule and inter-plane distance of 3.410 Å.

Overall, it is evident that the red polymorphs are based on pyrazine···pyrazine π-interactions with short inter-plane distances of 3.2–3.3 Å, whereas in the yellow modifications the pyrazine ring of one molecule is aligned with either an Au–S bond or a phenyl ring of a second molecule, with wider π–π distances of > 3.4 Å. There are no significant differences in the intramolecular distances and angles. All structures show the expected coordination environment around Au, except for the N-Au-S units which deviate significantly from linearity, with N-Au-S angles ranging from 170.7–175.7°. This effect is most probably due to steric repulsion between the *t*Bu substituents of the pincer ligand and the thiolate ligands; in S-pyridyl complex the intramolecular N···H interactions may be an additional distorting factor.

Intermolecular interactions in solution

To understand whether such interactions persist in solution, the self-aggregation tendency of **1** and **5** was explored by means of NMR spectroscopy. In particular, we investigated the concentration dependence of both the ^{1}H NMR spectrum and the self-diffusion coefficient (D_t) in CD_2Cl_2.

The results indicate that chemical shift values of both **1** and **5** are only marginally affected by increasing the concentration from 10^{-4} to over 10^{-2} M (see the Supporting Information). Protons H2 and H5 (for numbering see Scheme 1) showed the highest variability, which suggests the presence of head-to-head interactions arising from π-stacking of two pyrazine rings, as was observed in the solid state. In agreement with this assumption, the chemical shift values of the thiolate moieties were almost independent of concentration. By imposing a monomer-dimer equilibrium model, we derived rather small values of average dimerization constants $K_{dim} = 1.0$ and $1.8\ M^{-1}$ for **1** and **5**, respectively, suggesting that the concentration of π-stacked dimers in solution is low. This method suggests mol

fractions of dimers of around 10 mol% at [**1**] = 55.5 mM, and about 18 mol% in the case of [**5**] = 72.5 mM.

As independent confirmation of this association, self-diffusion coefficient values D_t of **1** and **5** were determined by diffusion NMR techniques[25] (see the Supporting Information for details). From the D_t values, the structural parameters *P* were derived by approximating the shapes of **1** and **5** to an oblate ellipsoid and plotted against the concentration. Also, in this case the *P* values were found to be slightly dependent on the concentration, as expected for a weak self-aggregation process. In good agreement with the interpolation of the chemical shift data, the concentration of dimers rises from 2 mol% at [**1**] = 2.9 mM to 21 mol% at [**1**] = 55.5 mM. Compound **5** showed a similar trend, with 2% dimers at 0.6 mM, rising to 26% at 72.5 mM (Supporting Information, Table S3.1). The chloride (C^N^{Pz}^C)AuCl was included in these measurements for comparison; it shows a similar tendency towards π-stacks in solution, which demonstrates that this aggregation is connected with the pincer structure, not the thiolate ligands.

Photophysical properties

The photophysical properties of these complexes depend on the structures of the crystal polymorphs in the solid state and on the formation of π-stacked aggregates in solution.

The UV/Vis absorption spectra of **1**–**9** show the expected pattern, with the typical low energy bands characterized by the vibronic progression of the C^N^C pincer ligands which are attributed to metal-perturbed ^{1}IL(C^N^C) transitions.

As is illustrated in Figure 4, in the pyridine complex (C^N^{py}^C)AuSNp-2 (**9**) this low energy band is significantly blue-shifted relative to the pyrazine analogue **5**; this shift reflects the fact that the π* level in pyrazine is 0.95 eV lower than in pyridine.[16] A comparison of the spectra of (C^N^{pz}^C)AuCl and **5** suggests that thiolato ligands slightly increase this π–π* energy gap.

Absorption maxima in the 420–440 nm region of the thiolates disagree with the observed deep-red colour of the pyrazine-based thiolate complexes in dichloromethane solution. The deep colour can however be explained by the weak broad absorption tail in the 470–530 nm region, ($\varepsilon \approx 1$–2×10^3 M^{-1}cm^{-1}; see the Supporting Information). Given the results of the NMR experiments, these low energy bands are most probably a reflection of molecular aggregation in solution.

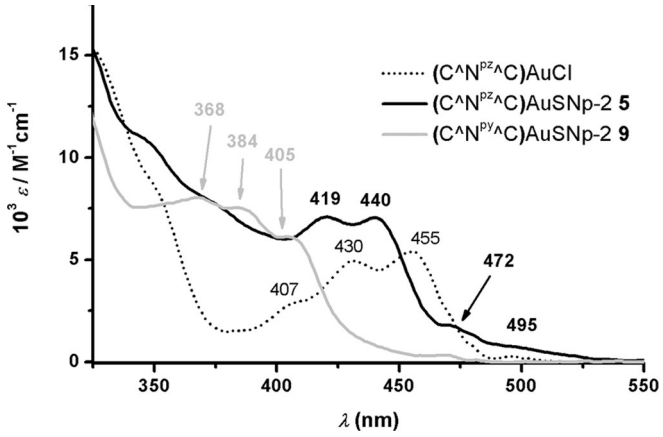

Figure 4. Comparison between the UV/Vis absorption spectra of (C^N^{pz}^C)AuCl, (C^N^{pz}^C)AuSNp-2 (**5**), and (C^N^{py}^C)AuSNp-2 (**9**) in CH_2Cl_2 (5×10^{-5} M).

The complexes show photoluminescence both in solution and in the solid state. The luminescence properties can be rationalized on the basis of two general emissive pathways: a green-centred emission, characterized by the vibronic progression due to the C=N stretching mode of the pincer ligand, of a type seen for many such C^N^C pincer complexes and attributed to a ^{3}IL(C^N^C) transition,[5,6] and a second, lower-energy unstructured red emission band at > 600 nm.

In the solid state at room temperature the complexes of N-heterocyclic aryl thiolates, that is, (C^N^{pz}^C)AuSC$_5$H$_4$N-2 (**3**) and (C^N^{pz}^C)AuSQuin-2 (**6**) are weakly to non-emissive, but on cooling to 77 K they show a green emission spectrum with vibronic structure. In solution and in PMMA matrix relatively weak green emissions are observed even at 298 K (Supporting Information, Tables S4.2 and S4.3). The same behaviour is seen for the 2,6-diphenylpyridine pincer complex **9**, which is emissive only at 77 K, with the ^{3}IL(C^N^{py}^C) band showing the typical structured profile with $\lambda_{em}^{max} = 517$ nm.

Nevertheless, compounds **3**, **6**, and **9** are the exceptions in this series of thiolato complexes given that complexes with aryl thiolates without hetero-ring atoms (**1**, **2**, **4**, and **5**), as well as the alkyl based 1-adamantylthiolate **8**, all show emissions dominated by unstructured red low-energy bands. Even more striking is the analysis of the excitation bands in both cases. While in **9** the excitation at 77 K resembles the absorption spectrum at 298 K, in the case of **5**, the emission at 298 K is associated with a fairly sharp low-energy excitation band at $\lambda_{ex} =$ 540 nm. This is also evident in the increase in emission quantum yield with increasing excitation wavelength, which reflects the shape of the excitation band. This points to the association of the red emission with the low-energy tail of more than 500 nm observed in the UV/vis spectrum; this band is therefore most probably connected with the pyrazine π-aggregation process described above. The two types of emissive behaviour are illustrated in Figure 5 for compounds **5** and **9**.

The relationship of the red emission with the type of π-stacking is further supported by the very different solid-state photoluminescence properties of the red and yellow crystal polymorphs **5 red** and **5 yellow**. While crystals of **5 red** show unstructured emission bands both at 298 and 77 K (λ_{max} 650 nm at 298 K, 653 nm at 77 K), **5 yellow** is non-emissive at 298 K, while at 77 K only the structured green ^{3}IL(C^N^{pz}^C) emission band is observed. Evidently the complex profile of the emission band of **5** isolated as a powder from the reaction mixture prior to recrystallization is the result of the sum of these two components (Figure 6a).

The two different emission pathways are also evident in solution and depend on concentration, temperature, and the solvent. For example, a 10^{-5} M dichloromethane solution of **5** shows the green triplet emission, which changes to red as the

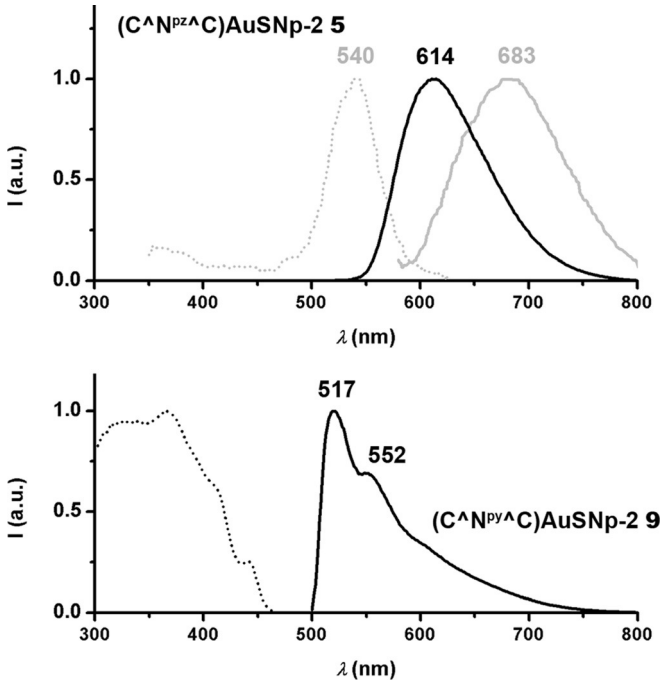

Figure 5. Top: Emission of **5** at 298 K (grey solid line; λ_{ex} 540 nm), excitation band at 298 K (grey dotted line), and emission at 77 K (black solid line; λ_{ex} 490 nm) (CH_2Cl_2, 10^{-4} M). Bottom: Emission of **9** at 77 K (λ_{ex} 400 nm; black solid line) and excitation band at 77 K (black dotted line; CH_2Cl_2, 10^{-4} M).

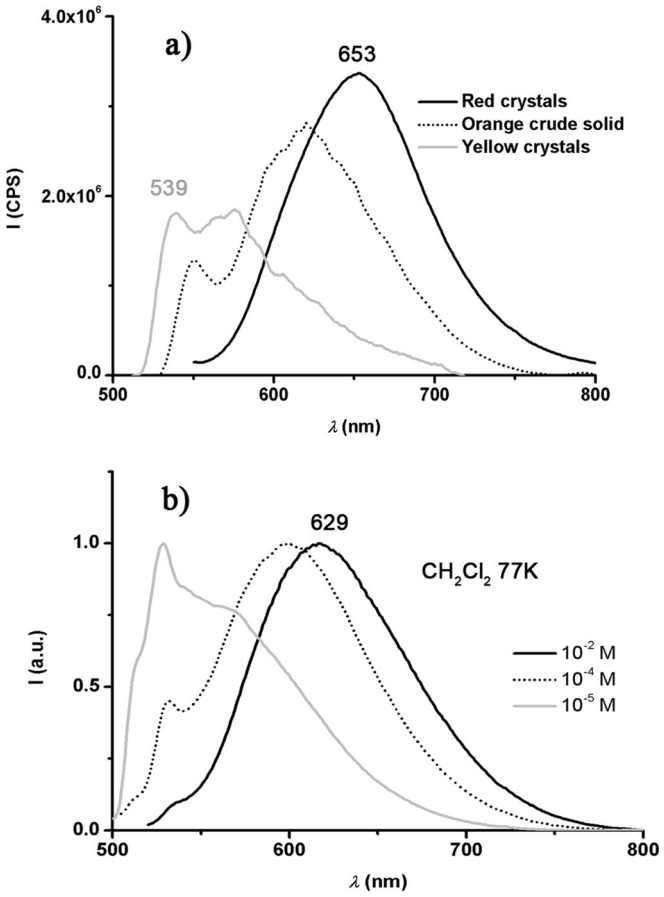

Figure 6. a) Photoemission spectra of crystalline samples of **5 red** (black solid line) and **5 yellow** (grey solid line) and the crude orange solid **5** (black dotted line) at 77 K. b) Normalized photoemission spectra of **5** in CH_2Cl_2 at different concentrations.

concentration increases (Figure 6 b). Another factor is the solvent: 10^{-2} M dichloromethane solutions of **2** and **5** at 77 K show red emissions, while in frozen 2-methyl-THF at the same concentration and temperature green structured bands are observed.

Even for the same sample the emission characteristics can be switched. A particularly striking case for the change of emission pathway as a function of sample history is provided by solutions of **2** (Figure 7). In frozen dichloromethane at 77 K complex **2** (10^{-2} M) produces the expected red emission; however, warming to just above the melting point of the solvent followed by refreezing leads to a mixed emission, orange to the naked eye. Repeating this cycle a number of times generates predominantly the structured green ^{3}IL(C^N^{pz}^C) emission, which on warming to 298 K reverts to red. All these findings confirm that the origin of the red emission is the π-aggregation of the pyrazine-based pincer ligands. Clearly the thaw–freeze treatment of the solution affects the concentration of π-stacked dimers and influences intermolecular interactions and the emission mode.

The complexes show a similar aggregation tendency when embedded in a polymer matrix, poly(methylmethacrylate) (PMMA). Varying the concentrations in PMMA demonstrates the fundamental differences in the green and red emission pathways. The photoluminescence quantum yield (PLQY) of the blue–green emitting quinolinyl thiolate complex **6** decreases with increasing concentration; by contrast, complex **5** shows an increase in PLQY from $\Phi_{PL} < 0.01$ at 1 wt% loading to $\Phi_{PL} = 0.11$ at 50wt% loading, together with a slight red-shift (Figure 8; Supporting Information, Tables S4.3, S4.4). The behaviour of **6** resembles the concentration-dependent quenching observed for the classical triplet emitter, Ir(ppy)$_3$.[26] The emission of **5**, by contrast, shows aggregation-induced PL enhancement.[27] The same trends in the emissions of **5** and **6** were observed in other polymers, such as polystyrene and PVK (polyvinyl carbazole).

Further information about the nature of the red emission is provided by the excitation lifetimes. The aggregation-induced red bands in the solid state and in a PMMA polymer matrix decay following bi-exponential functions (Supporting Information, Table S4.3); this was investigated in detail in the case of complex **5**.

The red band of **5** in PMMA is the result of two different components; a prompt emission with a short lifetime of 25–30 ns, which is assigned to photoexcited singlet states, and a delayed component with a temperature-dependent lifetime in the range of 0.3–20 μs (Figure 9). The emission band measured after 200–250 ns shows the same profile as the prompt emission (Supporting Information, Figure S35), suggesting that both emissions originate from states with similar energies. Despite the negligible effect of temperature on the emission wavelength, there is a strong dependence of the lifetime of

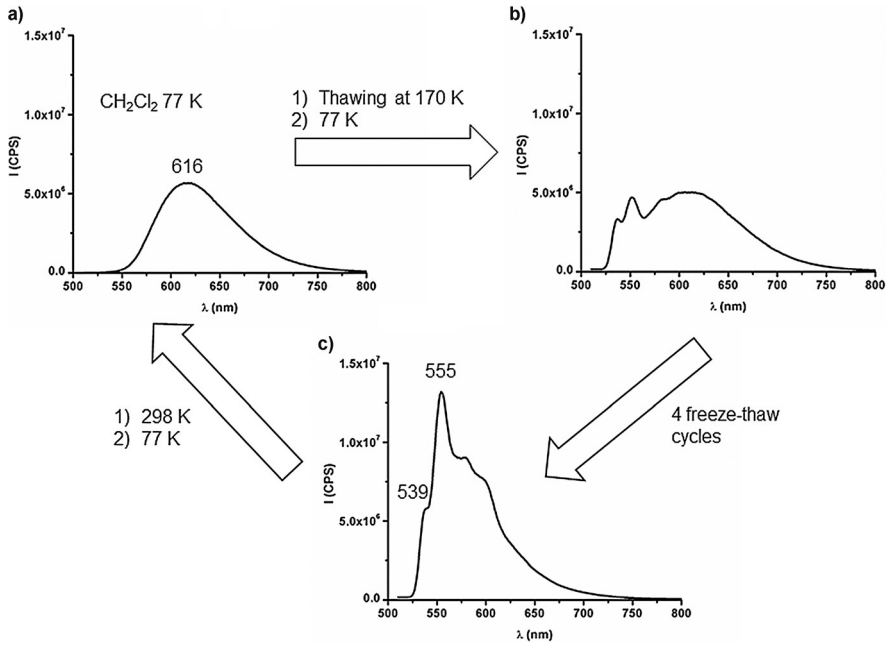

Figure 7. Changes in the emission spectra of CH_2Cl_2 solutions of **2** (10^{-2} M) with sample treatment. a) Initial spectrum at 77 K; b) spectrum after thawing at 170 K followed by cooling to 77 K; c) spectrum of **2** at 77 K after four freeze–thaw–freeze cycles.

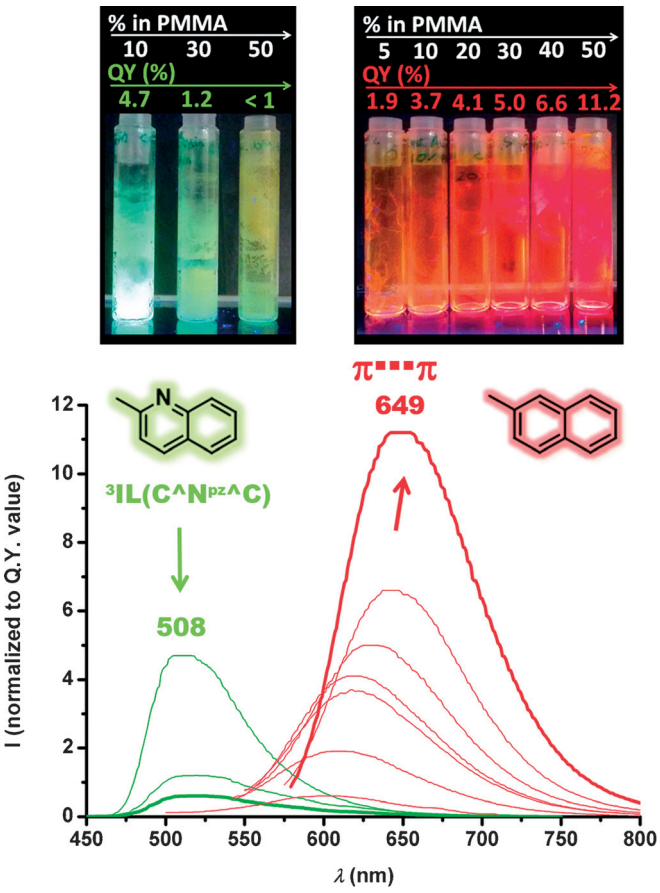

Figure 8. Changes in photoluminescence intensity as a function of concentration, showing the increase for **5** (red) and the decrease for **6** (green) in PMMA matrices with 5–50 wt%$^{-1}$ loading (298 K).

the long-lived component on temperature, with characteristic activation energy of 73 ± 5 meV. Since this longer-lived state constitutes the major emission component, there is a marked drop in luminescence intensity with increasing temperature (Supporting Information, Table S4.8 and Figure S36). This suggests a triplet parentage for the long-lived component, with triplet lifetime limited by typical thermally-promoted non-radiative decay.

In contrast to the behaviour in PMMA films, in solution at room temperature the red emission shows only the prompt mono-exponential decay, with a lifetime of 28 ns, suggesting the long-lived triplet-mediated emission component is fully quenched. In glassy conditions (solutions frozen to 77 K) the same effect as in polymeric matrix is observed, that is, the long-lived emission recovers, with lifetime in the μs regime.

Theoretical calculations

To support the analysis of the experimental data we have performed density functional (DFT) and time-dependent density functional theory (TDDFT) calculations with a particular focus upon providing insight into the influence of the type and magnitude of the supramolecular interactions in the photophysical properties of the complexes. Details of the calculations can be found in the Supporting Information. Complex **5** was selected as model for all the complexes. Specifically, three different structural dispositions have been optimised: an isolated molecule (**5 monomer**), a dimer based on the pz-pz aggregation of the red crystal (**5 reddimer**), and a dimer based on the S-pz aggregation of the yellow form (**5 yellowdimer**).

In all cases, the optimized structures agree with the X-ray analysis (Supporting Information, Table S5). This is not only il-

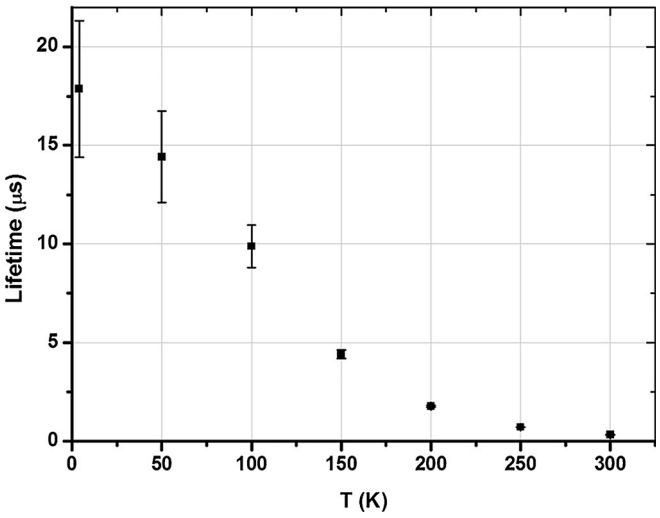

Figure 9. Variation of the excitation lifetime of the long-lived component of **5 red** in (10 wt%$^{-1}$ in PMMA film) at different temperatures.

lustrated by the intramolecular distances but also the distances between gold coordination planes, which fit the observed supramolecular arrangements in both dimers (**5 reddimer**: inter-plane distance 3.26 Å (calculated) vs. 3.235 Å (X-ray); **5 yellowdimer**: 3.45 Å vs. 3.482 Å (X-ray)).

The frontier orbitals of these limit situations show a particular relevant feature: whereas in **5 reddimer** the HOMO is mainly located on one thiolate ligands, the LUMO is delocalized over both pyrazine ligands (Figure 10). It is this bimolecular MO that is responsible for the intense, unstructured red photoemission.

By contrast, in **5 yellowdimer** the LUMO is located on the cyclometallated ligand of the same molecule, without delocalization over both molecules of the dimer. Very similar frontier orbitals are found in **5 monomer**, in line with the concept that

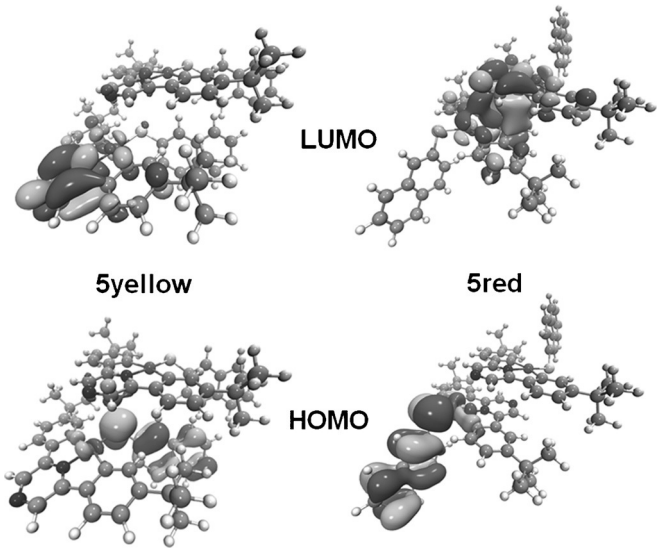

Figure 10. HOMO and LUMO frontier orbitals for **5 yellowdimer** and **5 reddimer**.

the photophysical properties of the yellow polymorphs are based on isolated molecules, not supramolecular aggregation.

The calculated emission energy for the optimised triplet geometry of **5 reddimer** is 1.76 eV (704 nm, oscillator strength 2×10^{-4}) which is in agreement with the red emission discussed above. In contrast, for **5 yellowdimer** and **5 monomer** the energy of this transition is very low (>850 nm), so the non-radiative emission rate will be large. The calculations suggest that the emission does not arise from this lowest triplet state but from the second triplet T_2 (λ_{em} (calcd) = 573 nm for **5 monomer** and 585 nm for **5 yellowdimer**). This transition is mainly HOMO−2→LUMO, and the nature of these orbitals confirms the $^3\pi$–π^*(C^N^{pz}^C) parentage.

The theoretical calculations support our interpretation of the experimental results. The green, structured emission has ^{3}IL(C^N^C) character and is based on isolated molecules; however, aggregation through pyrazine···pyrazine π-interactions, and only through pyrazine···pyrazine π-interactions, induces the appearance of a second emissive pathway. The origin for this emission is most probably charge-transfer transitions from the thiolate to the π-stacked dimeric pyrazine moiety, ^{3}LLCT(SR→{(C^N^{pz}^C)$_2$}). The presence of two components in rigid media (frozen solution or polymer matrix) and a single, red-shifted, emission in solution can be rationalized on the basis of two emissive states of very similar energy, which are able to relax in fluid conditions to a unique lower energy state.

Conclusion

In summary, gold(III) thiolato complexes based on cyclometallated pyrazine-centred pincer ligands form a new class of photoluminescent gold compounds, which are characterized by the remarkable dependence of their luminescence behaviour on the type of supramolecular arrangement present in the solid and in solution. Crystals of the aryl thiolates (C^N^{pz}^C)AuSR (R = Ph, 2-naphthyl) exhibit polymorphism and consist of a red, strongly photoemissive phase, and a yellow modification, which is non-emissive at room temperature. The deep red colour is associated with the formation of head-to-head π-stacked dimers in which pyrazine rings of neighbouring molecules adopt a "parallel offset" orientation. This disposition shows short inter-plane distances of 3.2–3.3 Å, compared to about 3.4 Å in the non-emissive modifications. NMR and UV/Vis spectroscopy confirmed that similar π-stacked dimers are also present in solution; this explains the concentration-dependent emission behaviour of these compounds. Changes in the π-interactions in solution, which can be brought about by freeze–thaw cycles, allow the emission characteristics to be switched reversibly between red and green.

While isolated molecules at 77 K show the typical green, vibronically structured emissions of ligand-based ^{3}IL(C^N^C) triplet transitions, calculations show that dimerization through pyrazine···pyrazine interactions produces a LUMO delocalized over the supramolecular π-dimer. This MO is involved in the bimolecular excited state and is mainly responsible for the observed red ^{3}LLCT(SR→(C^N^{pz}^C)$_2$) emission. While in PMMA matrix the green ^{3}IL(C^N^C) emission is subject to concentra-

tion quenching, the photoluminescence quantum yield of the red emission increases with increasing concentration. To the best of our knowledge this is first detailed study of aggregation-enhanced emission in Au^{III} chemistry.

Acknowledgements

This work was supported by the European Research Council. M.B. is an ERC Advanced Investigator Award holder (grant no. 338944-GOCAT). D.C. and S.J. acknowledge the Royal Society for financial support. We are grateful to the EPSRC National Crystallographic Service, Southampton, UK, for collection of crystallographic data sets.[29] We thank the Centro de Investigación en Síntesis Química, Universidad de La Rioja, E-26006, Logroño, Spain, and especially Professor E. Lalinde, for their kind assistance with the determination of the PL properties of the complexes.

Keywords: coordination chemistry · gold · photoluminescence · stacking interactions · supramolecular assembly · tridentate ligands

[1] Review: C. Bronner, O. S. Wenger, *Dalton Trans.* **2011**, *40*, 12409 – 12420.
[2] V. W.-W. Yam, K. M. C. Wong, *Chem. Commun.* **2011**, *47*, 11579 – 11592.
[3] C. Fan, C.-L. Yang, *Chem. Soc. Rev.* **2014**, *43*, 6439 – 6469.
[4] Review: D.-A. Roşca, J. A. Wright, M. Bochmann, *Dalton Trans.* **2015**, *44*, 20785 – 20807.
[5] a) W.-P. To, G. S.-M. Tong, W. Lu, C.-S. Ma, J. Liu, A. L.-F. Chow, C.-M. Che, *Angew. Chem. Int. Ed.* **2012**, *51*, 2654; *Angew. Chem.* **2012**, *124*, 2708; b) W.-P. To, K. T. Chan, G. S. M. Tong, C. S. Ma, W.-M. Kwok, X. G. Guan, K. H. Low, C.-M. Che, *Angew. Chem. Int. Ed.* **2013**, *52*, 6648; *Angew. Chem.* **2013**, *125*, 6780; c) G. Cheng, K. T. Chan, W.-P. To, C.-M. Che, *Adv. Mater.* **2014**, *26*, 2540; d) F.-F. Hung, W.-P. To, J.-J. Zhang, C.-S. Ma, W.-Y. Wong, C.-M. Che, *Chem. Eur. J.* **2014**, *20*, 8604 – 8614; e) G. S. M. Tong, K. T. Chan, X. Chang, C.-M. Che, *Chem. Sci.* **2015**, *6*, 3026.
[6] Recent examples: a) K. M.-C. Wong, L. L. Hung, W. H. Lam, N. Zhu, V. W.-W. Yam, *J. Am. Chem. Soc.* **2007**, *129*, 4350; b) V. K.-M. Au, K. M.-C. Wong, D. P.-K. Tsang, M.-Y. Chan, N. Y. Zhu, V. W.-W. Yam, *J. Am. Chem. Soc.* **2010**, *132*, 14273; c) V. K.-M. Au, K. M.-C. Wong, N. Zhu, V. W.-W. Yam, *Chem. Eur. J.* **2011**, *17*, 130 – 142; d) V. K.-M. Au, W. H. Lam, W.-T. Wong, V. W.-W. Yam, *Inorg. Chem.* **2012**, *51*, 7537; e) V. K.-M. Au, D. P. K. Tsang, K. M.-C. Wong, M.-Y. Chan, N. Zhu, V. W.-W. Yam, *Inorg. Chem.* **2013**, *52*, 12713; f) M.-C. Tang, C. K.-M. Chan, D. P.-K. Tsang, Y.-C. Wong, M. M.-Y. Chan, K. M.-C. Wong, V. W.-W. Yam, *Chem. Eur. J.* **2014**, *20*, 15233; g) M.-C. Tang, D. P.-K. Tsang, Y.-C. Wong, M.-Y. Chan, K. M.-C. Wong, V. W.-W. Yam, *J. Am. Chem. Soc.* **2014**, *136*, 17861; h) V. K.-M. Au, D. P.-K. Tsang, Y.-C. Wong, M.-Y. Chan, V. W.-W. Yam, *J. Organomet. Chem.* **2015**, *792*, 109; i) S. K.-L. Siu, C. Po, K.-C. Yim, V. K.-M. Au, V. W.-W. Yam, *CrystEngComm* **2015**, *17*, 8153 – 8162; j) D.-A. Roşca, J. Fernandez-Cestau, A. S. Romanov, M. Bochmann, *J. Organomet. Chem.* **2015**, *792*, 117 – 122.
[7] a) J. A. Garg, O. Blacque, K. Venkatesan, *Inorg. Chem.* **2010**, *49*, 11463 – 11472; b) J. A. Garg, O. Blacque, K. Venkatesan, *Inorg. Chem.* **2011**, *50*, 5430 – 5441; c) A. Szentkuti, M. Bachmann, J. A. Garg, O. Blacque, K. Venkatesan, *Chem. Eur. J.* **2014**, *20*, 2585 – 2596; d) T. N. Zehnder, O. Blacque, K. Venkatesan, *Dalton Trans.* **2014**, *43*, 11959 – 11972; e) A. Szentkuti, J. A. Garg, O. Blacque, K. Venkatesan, *Inorg. Chem.* **2015**, *54*, 10748 – 10760.
[8] a) D.-A. Roşca, D. A. Smith, M. Bochmann, *Chem. Commun.* **2012**, *48*, 7247 – 7249; b) D. A. Smith, D.-A. Roşca, M. Bochmann, *Organometallics* **2012**, *31*, 5988 – 5998.
[9] A. Herbst, C. Bronner, P. Dechambenoit, O. S. Wenger, *Organometallics* **2013**, *32*, 1807 – 1814.
[10] R. Kumar, A. Linden, C. Nevado, *Angew. Chem. Int. Ed.* **2015**, *54*, 14287 – 14290; *Angew. Chem.* **2015**, *127*, 14495 – 14498.
[11] J. Kalinowski, V. Fattori, M. Cocchi, J. A. G. Williams, *Coord. Chem. Rev.* **2011**, *255*, 2401 – 2425.
[12] D. A. K. Vezzu, J. C. Deaton, J. S. Jones, L. Bartolotti, C. F. Harris, A. P. Marchetti, M. Kondakova, R. D. Pike, S. Q. Huo, *Inorg. Chem.* **2010**, *49*, 5107 – 5119.
[13] K. M.-C. Wong, M. M.-Y. Chan, V. W.-W. Yam, *Adv. Mater.* **2014**, *26*, 5558 – 5568.
[14] A relatively close contact of 3.495 Å has been reported in a crystalline Au^{III} pincer complex and interpreted as an Au···Au interaction; however, the calculated interaction energy was less than 0.02 eV: W. Lu, K. T. Chan, S.-X. Wu, Y. Chen, C.-M. Che, *Chem. Sci.* **2012**, *3*, 752.
[15] J. Fernandez-Cestau, B. Bertrand, M. Blaya, G. A. Jones, T. J. Penfold, M. Bochmann, *Chem. Commun.* **2015**, *51*, 16629 – 16632.
[16] a) C. Walker, M. H. Palmer, A. Hopkirk, *Chem. Phys.* **1990**, *141*, 365 – 378; b) I. C. Walker, M. H. Palmer, *Chem. Phys.* **1991**, *153*, 169 – 187.
[17] M. C. Gimeno, A. Laguna, in *Comprehensive Coordination Chemistry II*, (Eds. J. A. McCleverty and T. J. Meyer), Elsevier, Amsterdam **2003**, vol. 6, p. 1058ff.
[18] Gold(III) thiolates with bridging thiolato ligands: a) H. W. Chen, C. Paparizos, J. P. Fackler, Jr., *Inorg. Chim. Acta* **1985**, *96*, 137; b) S. Wang, J. P. Fackler, Jr., *Inorg. Chem.* **1990**, *29*, 4404 – 4407; c) J. J. Garcia, M. L. Hernandez, H. Torrens, A. Gutierrez, F. del Rio, *Inorg. Chim. Acta* **1995**, *230*, 173 – 176.
[19] Anionic $[Au(SR)_4]^-$ complexes: a) U. Abram, J. Mack, K. Ortner, M. Müller, *J. Chem. Soc. Dalton Trans.* **1998**, 1011 – 1019; b) S. Watase, T. Kitamura, N. Kanehisa, M. Nakamoto, Y. Kai, S. Yanagida, *Acta Crystallogr. Sect. C* **2003**, *59*, m162 – m164; c) R. E. Bachman, S. A. Bodolosky-Bettis, C. J. Pyle, M. A. Gray, *J. Am. Chem. Soc.* **2008**, *130*, 14303 – 14310.
[20] Polynuclear $Au^{(I,III)}$ thiolates: a) O. Crespo, F. Canales, M. C. Gimeno, P. G. Jones, A. Laguna, *Organometallics* **1999**, *18*, 3142 – 3148; b) M. Bardají, M. J. Calhorda, P. J. Costa, P. G. Jones, A. Laguna, M. R. Perez, M. D. Villacampa, *Inorg. Chem.* **2006**, *45*, 1059 – 1068.
[21] Cyclometalated Au^{III} thiolates: a) M. A. Mansour, R. J. Lachicotte, H. J. Gysling, R. Eisenberg, *Inorg. Chem.* **1998**, *37*, 4625 – 4632; b) M. A. Cinellu, G. Minghetti, M. V. Pinna, S. Stoccoro, A. Zucca, M. Manassero, *J. Chem. Soc. Dalton Trans.* **1999**, 2823 – 2831; c) R. V. Parish, J. P. Wright, R. G. Pritchard, *J. Organomet. Chem.* **2000**, *596*, 165 – 176; d) W. Henderson, B. K. Nicholson, S. J. Faville, D. Fan, J. D. Ranford, *J. Organomet. Chem.* **2001**, *631*, 41 – 46; e) D. Fan, C.-T. Yang, J. D. Ranford, J. J. Vittal, P. F. Lee, *Dalton Trans.* **2003**, 3376 – 3381.
[22] K.-H. Wong, K.-K. Cheung, M. C.-W. Chan, C.-M. Che, *Organometallics* **1998**, *17*, 3505 – 3511.
[23] T. Zou, C. T. Lum, S. S.-Y. Chui, C.-M. Che, *Angew. Chem. Int. Ed.* **2013**, *52*, 2930 – 2933; *Angew. Chem.* **2013**, *125*, 3002 – 3005.
[24] Review: C. R. Martineza, B. L. Iverson, *Chem. Sci.* **2012**, *3*, 2191 – 2201.
[25] a) A. Macchioni, G. Ciancaleoni, C. Zuccaccia, D. Zuccaccia, *Chem. Soc. Rev.* **2008**, *37*, 479 – 489; b) L. Rocchigiani, A. Macchioni, *Dalton Trans.* **2016**, *45*, 2785 – 2790.
[26] S. Takayasu, T. Suzuki, K. Shinozaki, *J. Phys. Chem. B* **2013**, *117*, 9449 – 9456.
[27] In the present case, individual molecules will show triplet emission. This process differs therefore from the well-recognized aggregation-induced enhancement (AIE) where aggregation limits molecular mobility so that aggregates of individually non-emissive molecules become luminescent: a) J. Mei, Y. Hong, J. W. Y. Lam, A. Qin, Y. Tang, B. Z. Tang, *Adv. Mater.* **2014**, *26*, 5429 – 5479; b) Z. Zhao, B. Hea, B. Z. Tang, *Chem. Sci.* **2015**, *6*, 5347 – 5365.
[28] CCDC 1495509 (**1 red**), 1495510 (**1 yellow**), 1495511 (**2**), 1495512 (**3**), 1495513 (**5 red**), 1495514 (**5 yellow**), 1495515 (**7**), and 1495516 (**9**·CH_2Cl_2)) contain the supplementary crystallographic data for this paper. These data can be obtained free of charge from The Cambridge Crystallographic Data Centre.
[29] S. J. Coles, P. A. Gale, *Chem. Sci.* **2012**, *3*, 683 – 689.

Received: August 11, 2016
Published online on November 9, 2016

